ChemCatChem

The European Society Journal for Catalysis

Chemistry Europe

European Chemical Societies Publishing

Supported by GECATS GERMAN CATALYSIS SOCIETY

Accepted Article

Title: High-Performance Supported Ru Catalysts for the Aqueous-Phase Hydrogenation of Levulinic Acid to γ-Valerolactone

Authors: María S. Leguizamón-Aparicio, Juan José Musci, Maia Montaña, Leticia J. Méndez, María L Barbelli, Elena Rodríguez-Aguado, Juan A Cecilia, Enrique Rodríguez-Castellón, Ileana D. Lick, and Monica Laura Casella

To be cited as: *ChemCatChem* **2024**, e202301719

Link to VoR: https://doi.org/10.1002/cctc.202301719

WILEY VCH

RESEARCH ARTICLE WILEY-VCH

High-Performance Supported Ru Catalysts for the Aqueous-Phase Hydrogenation of Levulinic Acid to γ-Valerolactone

María S. Leguizamón-Aparicio[a], Juan J. Musci[b,c], Maia Montaña[d], Leticia J. Méndez[a], María L. Barbelli[a], Elena Rodríguez-Aguado[d], Juan A. Cecilia[d], Enrique Rodríguez-Castellón[d], Ileana D. Lick*[a], Mónica L. Casella*[a][b]

[a] Dr. M.S. Leguizamón-Aparicio, Dr. L.J. Méndez, Dr. M.L. Barbelli, Prof. Dr. I.D. Lick, Prof. Dr. M.L. Casella
Centro de Investigación y Desarrollo en Ciencias Aplicadas "Dr. Jorge J. Ronco" (CINDECA) (CCT CONICET-La Plata), Universidad Nacional de La Plata and Comisión de Investigaciones Científicas (CIC). Calle 47 No. 257, 1900 La Plata, Argentina
E-mail: ilick@quimica.unlp.edu.ar (IDL); casella@quimica.unlp.edu.ar (MLC)
[b] Dr. J. J. Musci, Dra M. L. Casella
Departamento de Ciencias Básicas y Experimentales
Universidad Nacional del Noroeste de la Provincia de Buenos Aires
Roque Saenz Peña 456, (6000) Junín –Argentina
[c] Dr. J. J. Musci
Centro de Investigaciones y Transferencia del Noroeste de la Provincia de Buenos Aires (CITNOBA) – UNNOBA-UNSAdA-CONICET
Monteagudo 2772, (2700) Pergamino, Argentina
[d] Dr. M. Montaña, Dr. E. Rodríguez-Aguado, Dr. J.A. Cecilia, Prof. Dr. E. Rodríguez-Castellón
Departamento de Química Inorgánica, Cristalografía y Mineralogía (Unidad Asociada al ICP-CSIC), Facultad de Ciencias, Universidad de Málaga
Campus de Teatinos, 29071 Málaga, Spain

Supporting information for this article is given via a link at the end of the document.

Abstract: γ-Valerolactone (GVL) can be obtained by efficient hydrogenation of levulinic acid using ruthenium-based catalysts in an aqueous medium. This paper reports an in-depth study on the activity and selectivity of Ru catalysts supported on zirconia-alumina, focusing on the effect of Ru concentration (0.5, 1.5 and 3 wt.% of Ru) and the selection of operational reaction variables. The results showed that the activity strongly depends on the number and oxidation state of the supported ruthenium particles. The most active catalyst, Ru3/ZA, presented the highest number of nanometric particles of zerovalent Ru and the highest number of acid sites. This catalyst gave ca. 100% selectivity towards GVL, at high conversion of levulinic acid (over 99%) under the best operating conditions evaluated (120°C, 3 MPa H_2 pressure, 1 h of reaction, and 0.1 g of catalyst). In addition, this catalyst kept high levels of conversion and selectivity after successive reuse cycles.

Introduction

Fossil resources are finite, and their demand is continually increasing. For this reason, in addition to a growing awareness of climate change, in recent decades the scientific community has focused on the search for alternative energy sources (wind, hydrogen, solar, etc.), as well as the substitution of petrochemical products by others from renewable sources.

A sustainable carbon source comes from lignocellulosic biomass, composed mainly of polymeric hydrocarbon chains: cellulose, hemicellulose, and lignin. Cellulose is a biopolymer composed of glucose molecules, hemicellulose is composed of sugars with 5 and 6 carbons, and lignin is a three-dimensional network structure formed by the connection of polyphenols. In this sense, it should be clarified that although lignocellulosic biomass is widely used to obtain food, there is a considerable amount of it that is discarded as waste. The processing of the residual biomass, whose composition varies depending on the original substrates, has been approached using different types of processes (thermochemical, chemical-hydrolytic, and biological). All the proposed strategies involve stages for obtaining sugar monomers and/or their derivatives through various reactions (depolymerization, isomerization, hydrolysis, dehydration, rehydration, etc.). (Scheme 1).[1]

The products obtained by the different processes are called biomass-based platform compounds, which include sugar monomers, furanic compounds (5-hydroxymethyl furfural and furfural), alcohols, lactic acid, and levulinic acid, among others.

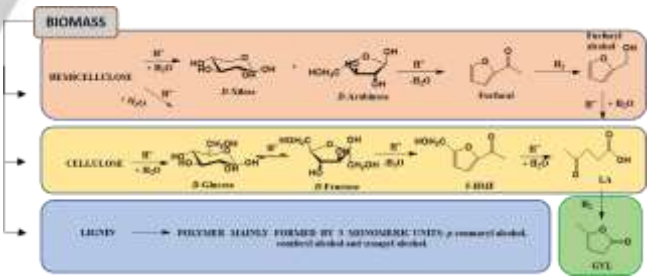

Scheme 1. Schematic representation of biomass-based platform compounds obtained through depolymerization, isomerization, hydrolysis, dehydration, rehydration, etc. (adapted from [1]).

From these compounds it is possible to obtain others with higher added value, thus developing new synthesis routes and processes that have given rise to the so-called lignocellulosic biorefinery. [2,3,4,5]

The US Energy Agency has considered that one of the 12 platform molecules that exhibits great potential for obtaining compounds with high added value is levulinic acid (LA).[6,7] LA contains two reactive functional groups in its structure, a carboxylic group, and a keto-carbonyl group. Different families of compounds can be obtained from LA by the reaction of these functional groups. Among the interesting synthesis products,

levulinate esters, alcohols, cycloesters such as angelica lactone and γ-valerolactone can be mentioned. One of the LA derivatives that has received considerable attention in the last decade is γ-valerolactone (GVL) since this product can be used as a potential liquid fuel, food additive, and fuel additive. This compound also has key physicochemical properties to be considered a green and safe solvent. It is stable and does not form peroxides at 60°C, is nontoxic, has a high boiling point, low melting point, and low vapor pressure, and can solubilize a large number of compounds and has the advantage of being biodegradable and bioremediable. On the other hand, it is a precursor for valuable chemicals such as methyl tetrahydrofuran, 1,4-pentane diol, and alkanes.[8,9,10]

In general, two mechanisms are proposed to explain the preparation of GVL from LA (Scheme 2).[11]

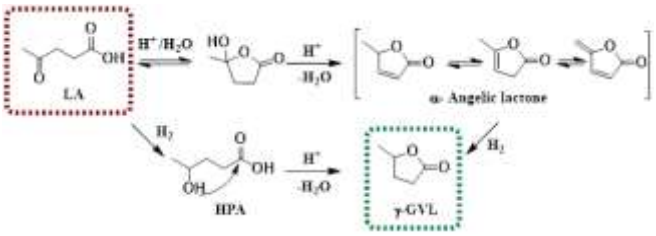

Scheme 2. Mechanisms proposed to explain the obtention of GVL from LA

One of them proposes, as a first step, the hydrogenation of the keto-carbonyl group of LA, which leads to the formation of an unstable intermediate, 4-hydroxypentanoic acid. Subsequent dehydration of this intermediate is followed by intramolecular esterification involving a cyclization to GVL.[12] According to thermodynamic and kinetic studies, this mechanism is dominant at low temperatures. In addition, there are bibliographic reports where the presence of 4-hydroxypentanoic acid has been demonstrated.[13,14,15] According to the second of the proposed mechanisms, the reaction begins with the dehydration of LA to give α-angelica lactone and the subsequent hydrogenation of its keto-carbonyl group to give GVL.[16,17] Some reports indicate that this reaction mechanism predominates at high temperatures or in the vapor phase.[11,13] Both proposed mechanisms have in common that the hydrogenation step is catalyzed by a metallic phase, while acid sites would be needed to accelerate the dehydration and cyclization steps.[18]

Levulinic acid can be converted to GVL using three sources of hydrogen: external molecular hydrogen, formic acid decomposition, or the Meerwein-Ponndorf-Verley reaction (MPV)[19]. Formic acid is an attractive alternative, but higher reaction temperatures are needed to decompose formic acid (H_2 + CO_2) and then hydrogenate LA[20]. In addition, the formation of CO through hydration decomposition of formic acid could poison the metal particles and deactivate the catalysts[21]. MPV requires mild conditions, but by-products decrease selectivity [22] On the other hand, hydrogenation using molecular hydrogen and heterogeneous catalysts offers easy liquid product separation, and is the most commonly used process for the hydrogenation of LA with metal catalysts in the aqueous phase. Several homogeneous and heterogeneous noble or non-noble metal catalysts have been reported to be active for the reaction.[1,13,23] In the case of homogeneous catalysts, various complexes have shown activity, and particularly with some ruthenium complexes remarkably high activity has been obtained. However, the disadvantage of these homogeneous systems is the difficulty of separating and recovering the catalysts. Regarding the heterogeneous systems used, in recent years, active phases based on the use of non-noble metal catalysts have been reported, mainly those that contain copper or nickel in their composition. In a recent review, Dutta et al. summarized the results found with this type of catalyst, as well as the operating conditions used.[23] In general, some of these catalysts have good activity under acceptable operating conditions; however, the use of these non-noble-based catalysts when water is the solvent should still be studied more extensively.

Among the heterogeneous systems based on the use of noble metal catalysts, those containing palladium and ruthenium are among the most active for the hydrogenation of the C=O bond.[24] In particular, ruthenium-based catalysts have the advantage of being active and selective in the aqueous phase and under operating conditions (pressure and temperature) that can be considered not so severe.[25,26,27] An important aspect to consider is that some ruthenium catalysts have high stability in the aqueous phase depending on the chosen support. In this sense, it has been proposed that the use of zirconia or titania favors the stability of the catalytic systems. In addition, the particle size of the supported metal phase, as well as its dispersion, strongly depends on the characteristics of the support used.[28,29,30] The dispersion of the active phases is an important factor to consider given that some authors have proposed that the reaction to obtain GVL from LA is sensitive to the size of the metallic particles. Thus, for example, Piskun et al.[31] obtained high activity in the conversion of LA to GVL with a titania-supported ruthenium catalyst having a ruthenium particle size of 2.2 nm. Similar results were found by X. Liu et al. with ruthenium-impregnated N-doped carbon sphere catalysts.[32] These authors showed that the activity increased substantially with increasing dispersion of the supported ruthenium nanoparticles (around 2.3 nm in size). The oxidation state of Ru could also play an important role, since Ru(0) nanoparticles are supposed to be the catalytically active species,[31] although an active role of the oxidized RuO_2 species in the catalytic cycle cannot be ruled out.

Another aspect that must be considered when choosing the support is its ability to supply the acid sites necessary for the dehydration and cyclization steps mentioned above, making the systems bifunctional. In this context, alumina is a widely used support in catalysis since it has a high specific surface area (150-200 m^2/g), which allows a good dispersion of the supported phases; it also has a certain amount of acidity and an incomplete spinel structure. This crystalline structure could favor the diffusion of the supported metallic phases into the lattice, reducing their surface availability and/or generating highly interacting species. That is why a modification of the alumina surface by adding other oxides, for example, zirconia, is sometimes proposed. The choice of zirconia is based on the fact that it presents polymorphs with controllable acid-base properties, good thermal stability, and a more closed crystal structure than that of gamma alumina.[33]

On these bases, this work reports on the activity and selectivity of ruthenium catalysts supported on a zirconia-modified alumina for the catalytic hydrogenation reaction of LA to give GVL. To compensate for the low solubility of H_2 in water, a highly active and selective metal catalyst is needed to carry out this reaction using molecular hydrogen as the reducing agent. In addition, due to the chemical environment in which this reaction takes

place, it is desirable for the catalyst to be highly stable. In particular, the catalytic system selected must be able to withstand the corrosiveness of the LA. Otherwise, there would be leaching of the metal and so deactivation of the catalyst. Based on these considerations, a series of catalysts with varying concentrations of ruthenium supported on alumina and zirconia-modified alumina were prepared. Specifically, the performance of the catalysts towards the production of GVL in aqueous phase was studied, changing different reaction variables (hydrogen pressure, temperature, and mass of catalyst). In addition, characterization and stability results after several reuse cycles are presented for the catalyst that turned out to be the most active.

Results and Discussion

Catalytic hydrogenation of LA

The aqueous phase catalytic hydrogenation of levulinic acid was evaluated using a series of catalysts prepared with variable concentration of ruthenium, Rux/ZA. The experimental conditions selected for this study were: T= 120°C, a constant H_2 pressure of 30 bar, a mass of catalyst of 0.1 g, and an initial LA concentration of 0.6 M. Figure 1 shows the results achieved with the series of Rux/ZA catalysts, both for the conversion of LA (Fig. 1a), and for the selectivity towards GVL as a function of time (Fig. 1b).

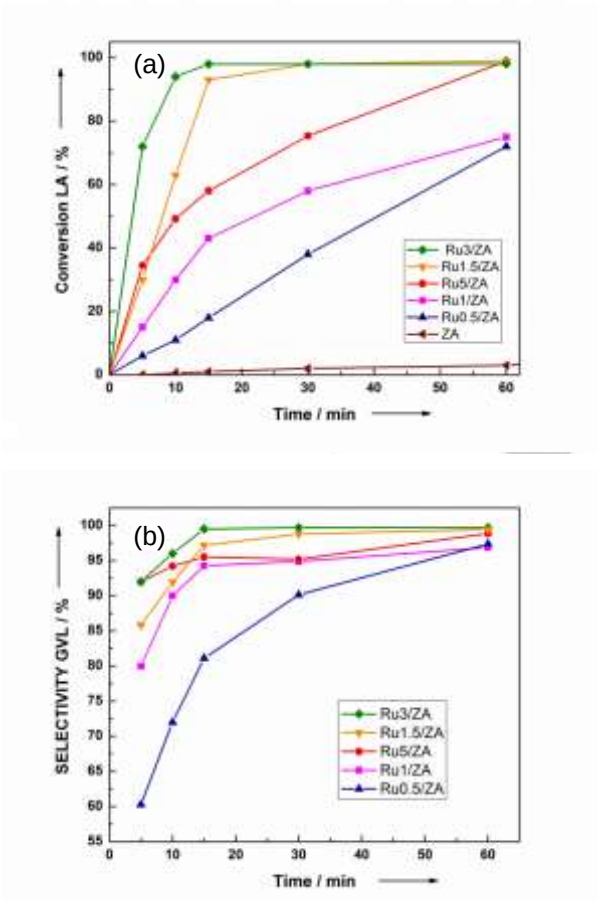

Figure 1. Conversion of LA (a) and selectivity to GVL (b) for the series of studied Rux/ZA catalysts.

Under the conditions used and during the entire course of the reaction, the support presented a practically negligible LA conversion, while the ruthenium-containing catalysts showed a very good activity. These results indicate the obvious crucial role of Ru in hydrogenation and also that the activity depends on the ruthenium content. Thus, the conversion of LA after one hour of reaction increased from 70% to 99% with increasing ruthenium content from 0.5 to 3 wt.%. Both Ru1.5/ZA and Ru3/ZA catalysts reached an almost complete conversion (~99%) at low reaction times (*ca.* 30 min). Increasing the ruthenium concentration up to a level of 5 wt.% results in a less active catalyst, which achieves less than 70% conversion after 0.5 h of reaction. From these results it can be concluded that the Ru3/ZA catalyst is the most active of all the catalysts studied. Tan et al*.* reported similar results with zirconia-supported ruthenium catalysts. These authors found that by increasing the ruthenium concentration from 0.5 to 2 wt.%, the conversion changed from 80.3% (3 h of reaction) to 100% (0.5 h of reaction) at a temperature of 130°C. me, indicating that a 2 wt.% Ru content was enough to provide the number of active sites to complete the reaction.[34]. To elucidate the activity-promoting properties of the catalysts, the characterization results of the most active catalysts, Ru1.5/ZA and Ru3/ZA, and the least active catalyst, Ru0.5/ZA, are presented below.

Support and catalyst characterization

The zirconia-alumina (ZA) support was prepared by depositing a zirconia hydrogel on a 252 m^2/g commercial γ-alumina to obtain a concentration of 15 wt.% ZrO_2 in the final support. After a thermal calcination process at 600°C, the zirconia-alumina system presented a surface area of 166 m^2/g, while the starting alumina calcined at the same temperature presented an area of 182 m^2/g. Textural properties of the supports are summarized in Table 1. The adsorption/desorption isotherms obtained for the alumina and the ZA support are included in the Supplementary Material (Figure S1). The ZA support exhibited a type IV isotherm according to the classification established by IUPAC[35], with the characteristic hysteresis of mesoporous materials, where the adsorption behavior is determined by the interactions between ZrO_2 and alumina. A bulk ZrO_2 material, prepared following a procedure analogous to that used in this work, exhibited a low surface area (73 m^2/g).[36] It is evident that the lower surface area found for the ZA support compared to the calcined alumina is due to a slight blockage of the pores of the alumina when dispersing the zirconia on it.

Table 1. Textural properties of the supports: Surface area, pore volume, and pore diameter.

Support	Surface area (m^2/g)	Pore volume (cm^3/g)	Pore diameter (A)
Calcined alumina	182	0.40	74
ZA	166	0.43	96

To obtain the best activation temperature of the ruthenium phases in the Rux/ZA catalysts, the precursors were subjected

to a reduction pretreatment under an $H_{2(g)}$ atmosphere. This temperature was obtained through temperature-programmed reduction (TPR) experiments. Fig. 2 shows the reduction profiles obtained for the studied Rux/ZA catalysts.

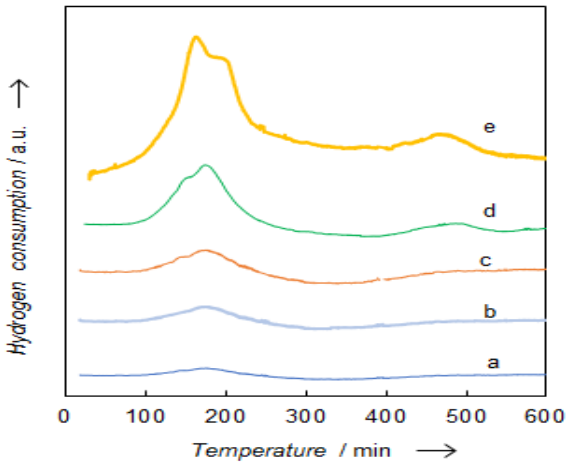

Figure 2. H_2-TPR profiles of a) Ru0.5/ZA; b) Ru1/ZA, c) Ru1.5/ZA; d) Ru3/ZA and e) Ru5/ZA

The reduction peak of Ru(III) to Ru(0) occurs between 75 and 250°C with a maximum at 180°C for three catalysts. In addition, this signal presents a shoulder at a lower temperature that could be associated with the reduction of more oxidized ruthenium species (Ru(IV)) or with ruthenium species with less interaction with the support. Besides, the TPR profiles present a second and weaker peak around 350–550°C, which could indicate the presence of ruthenium species that strongly interact with the support.[37] This signal is more intense in the reduction profile of the Ru3/ZA catalyst. According to the obtained results, 300°C was selected as the reduction temperature. Thermal treatment with pure H_2(g) for 2 h at this temperature would ensure complete reduction of ruthenium.

SEM-EDS, XRD, TEM-STEM, XPS studies and acidity measurements were carried out on the selected Rux/ZA catalysts to figure out their physicochemical properties. Fig. 3 shows the morphology of the catalysts as obtained by SEM. It can be seen that increasing the ruthenium content leads to the formation of new surface phases.

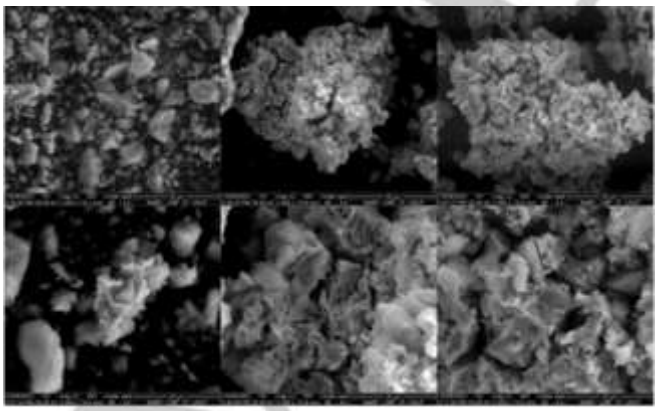

Figure 3. Ru0.5/ZA (left), Ru1.5/ZA (middle), and Ru3/ZA (right) catalyst morphology determined by SEM at two magnification levels: 2000X (upper part of the figure) and 5000X (lower part of the figure)

Besides, with the aim of obtaining information about the distribution and concentration of the phases present in the catalysts, mapping and semiquantitative chemical analysis of the elements that constitute the catalysts (Ru, Al, Zr) were conducted using the EDS technique. Element mapping indicates that both the zirconia and ruthenium phases are well distributed over the surface (see Supplementary Material, Fig. S2). For the chemical analyses by EDS, obtained over wide areas of analysis, the atomic mass ratios Zr/Ru and Al/Zr were calculated. These ratios were calculated assuming all the ruthenium was in its reduced state and the zirconium was in the form of ZrO_2. The catalysts have an Al/Zr atomic ratio slightly higher than nominal, indicating that a similar amount of zirconia has been deposited on the alumina as expected (Table 2). Nevertheless, it is worth mentioning that some specific analyses, in areas where the photoemission denoted a higher concentration of the zirconium element, gave an exceptionally low Al/Zr ratio, corresponding to small areas with ZrO_2 agglomerates.

Table 2. Ru mean particle size (measured by TEM), nominal composition, and chemical composition obtained by EDS.

	d_{TEM} (nm)	Nominal atomic ratio		Experimental atomic ratio[a]	
		Zr/Ru	Al/Zr	Zr/Ru	Al/Zr
ZA	----	----	13.69	----	16.5
Ru0.5/ZA	2.5	24.64	13.69	26	16.8
Ru1.5/ZA	2.7	8.13	13.69	9.55	15.3
Ru3/ZA	2.4	4.00	13.69	7.3	14.9 and 6.8

[a] by SEM-EDS

On the other hand, the Zr/Ru ratio found for the catalysts is somewhat higher than expected. These results may indicate that the ruthenium content in a surface layer of 100 μm thickness (microprobe penetration depth) is slightly lower than expected in the three samples, probably because part of the ruthenium is found as oxide. It should be noted that the results obtained in different areas of the samples are similar to each other, indicating that the samples have a homogeneous distribution of the supported ruthenium phase, except in those small Zr-enriched areas where the Zr/Ru ratio is much lower than expected (6.8).

In order to identify the crystalline ZrO_2 supported phases and the metallic ruthenium phases in the Ru-containing catalysts, XRD analyses were carried out. The obtained diffraction patterns are presented in Fig. 4. The broad diffraction signals, typical of transitional alumina, are seen at 66.8 and 45.8° (JCPDS Card No. 29–1480). In the pattern of ZA support and ruthenium-containing catalysts, the lines corresponding to the metastable tetragonal zirconia phase located at 2θ =30.5, 35.2, and 50.7° (PDF:01-089-7710) appear with very low intensity, which may indicate that ZrO_2 crystals have a very small size or are widely dispersed on the alumina surface. Furthermore, no diffraction peaks attributed to metallic Ru species are observed. This is probably because the particles are smaller than the adequate size to be identified by this technique.

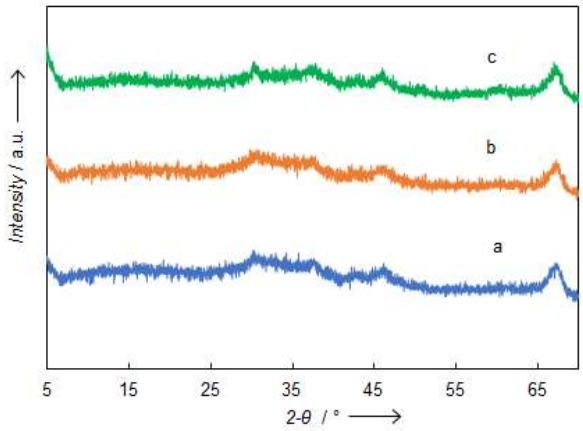

Figure 4. XRD patterns for a) Ru0.5/ZA; b) Ru1.5/ZA, and c) Ru3/ZA catalysts

To analyze whether the distribution of the species supported on the surface is homogeneous at the nanometric level, chemical mappings were performed using the scanning transmission and transmission electron microscopy (STEM and TEM) techniques. As observed by SEM-EDS, the results obtained with STEM suggest that both zirconia and ruthenium are well distributed on the catalytic surface, with the few exceptions where Zr enrichment is observed at the nanometric level. Fig. 5 shows the images of the STEM mappings of the Ru3/ZA catalyst as an example. Images of the other two catalysts are presented in the Supplementary Material (Fig. S3).

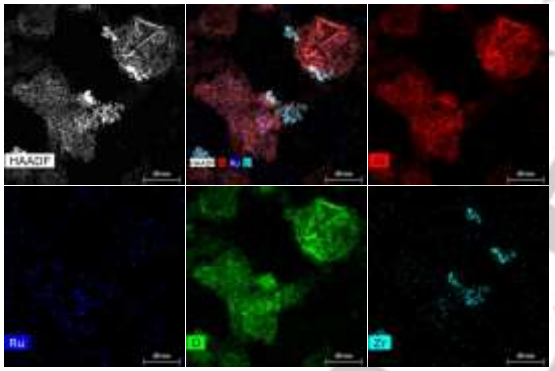

Figure 5. Elemental mappings performed by STEM on the Ru3/ZA catalyst.

Representative TEM images of the catalysts are presented in Fig. 6. The metallic particle size distributions obtained from TEM are also shown in Fig. 6. The micrographs corresponding to Ru0.5/ZA, Ru1.5/ZA and Ru3/ZA show the presence of highly dispersed ruthenium particles with diameters between 1.5 and 5 nm. The results obtained for the mean particle size are listed in Table 2. The increase in the ruthenium concentration does not generate an appreciable increase in the average particle size; it only slightly increases the number of larger particles.

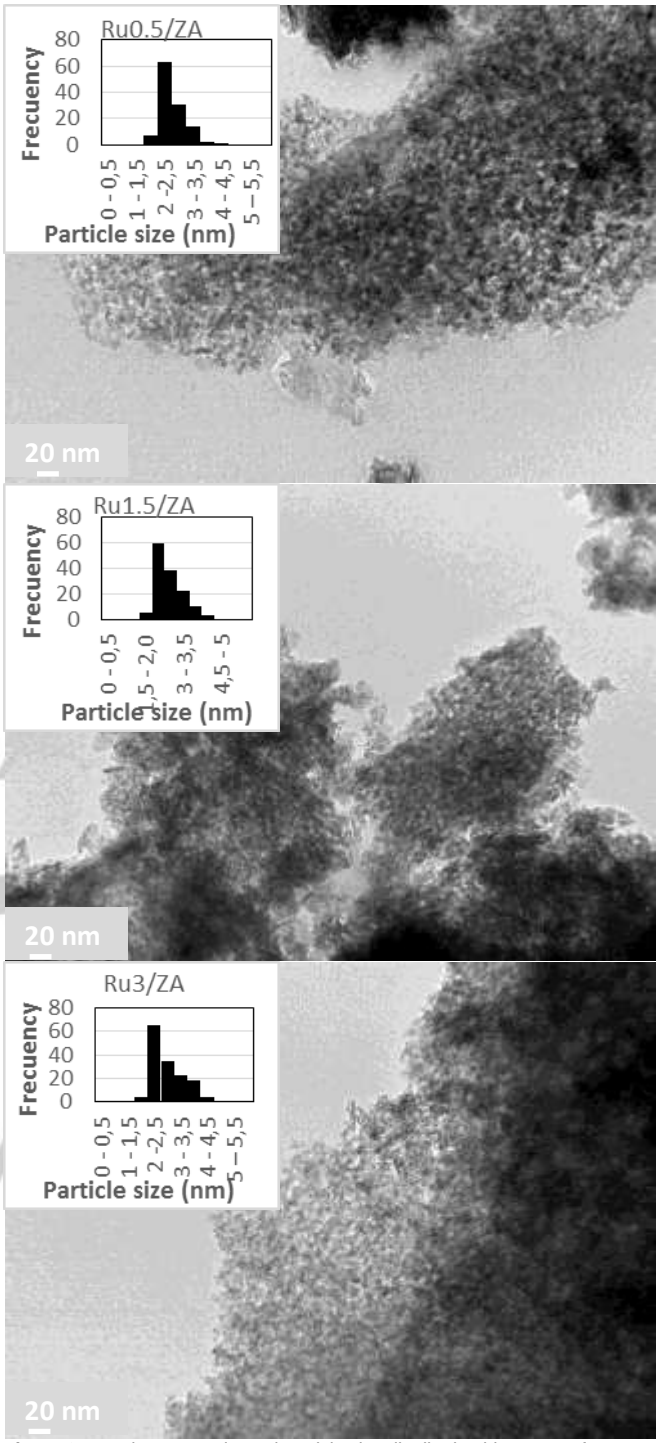

Figure 6. TEM images and metal particle size distribution histogram of Ru0.5/ZA, Ru1.5/ZA, and Ru3/ZA catalysts.

XPS analyses of the catalysts were performed to analyze the surface composition of the samples and the Ru oxidation state. The binding energies (BE) of the C 1*s*, Al 2*p*, Zr 3$d_{5/2}$, O 1*s*, Ru 3$d_{5/2}$, and Ru 3$p_{3/2}$ signals are included in Table 3. The analysis of ruthenium was conducted using the Ru 3$p_{3/2}$ region because part of the Ru 3*d* signal overlaps with that of C 1*s* signal. The spectra obtained for the Ru 3$p_{3/2}$ region are shown in the Supplementary Material (Fig. S4). The Al 2*p* peak appears at 74.5 eV, while the Zr 3$d_{5/2}$ was found at 182.4 eV. These values show that both elements are in their oxidized forms (Al(III) and Zr(IV))[38].

On the other hand, from the analysis of the spectra of the Ru $3p_{3/2}$ region (Fig. S4) it is inferred that the asymmetric signals found in the samples are associated with the coexistence of oxidized ruthenium species (Ru(III) and Ru(IV)) and metallic Ru phase.[39] The contributions assigned to Ru(0), Ru(III) and Ru(IV) appeared at *ca.* 461-462 eV, 463-464 and 465-466, respectively, upon deconvolution of the Ru $3p_{3/2}$ signals. Table 3 includes, in brackets, the percentage contribution of each of these species for each sample. From the results obtained, it is evident that the metallic ruthenium phase is the predominant one in all the studied catalysts. Besides, with increasing concentration, the proportion of metallic ruthenium decreases. This effect is remarkable for Ru3/ZA and Ru5/ZA catalysts, for which an increase in the proportion of Ru(IV) species was also found. This species presents a higher BE value than that observed for catalysts with a lower metal loading, indicating a higher interaction with the support and less availability, according to the results observed by TPR.

Table 3. Core level BE (eV) of Ru $3d_{5/2}$, Ru $3p_{3/2}$, C1*s*, O 1*s*, Al 2*p* and Zr $3d_{5/2}$

Catalyst	Ru $3d_{5/2}$	Ru $3p_{3/2}$	C1*s*	O 1*s*	Al 2*p*	Zr $3d_{5/2}$
Ru0.5/ZA	280.3	Ru (0) 461.8 (80) Ru (III) 463.1 (18) Ru (IV) 465.2 (2)	284.8	531.1	74.3	181.8
Ru1.5/ZA	280.5	Ru (0) 461.8 (75) Ru (III) 463.7 (17) Ru (IV) 466.9- (8)	284.8	531.1	74.3	181.7
Ru3/ZA	280.4	Ru (0) 461.9 (73) Ru (III) 464.4 (22) Ru (IV) 466.3 (5)	284.8	531.0	74.3	181.9
Ru5/ZA	280.4	Ru (0) 461.8 (71) Ru (III) 464.3 (24) Ru (IV) 466.2 (5)	284.8	531.1	74.3	181.8

From the quantitative analyses summarized in Table 4, it can be seen that as the ruthenium content increases, the surface ruthenium content increases. Moreover, there is a very good correlation between the nominal (theoretical) ruthenium content and the experimentally obtained Ru/Zr ratio (Fig. S5). The Ru/Zr ratio increases linearly as the Ru concentration increases from 0.5 to 3 wt.%. However, this linear correlation is lost at higher Ru contents (5 wt.%). It is evident that some ruthenium phases are segregated on the surface of the Ru5/ZA catalyst and thus there is a loss of metal phase dispersion. On the other hand, it is worth noting that the total surface ruthenium content is higher than the bulk value. It is evident that ruthenium is preferentially located on the catalytic surface during the impregnation process and that the low temperature chosen for the reduction treatment (300°C) does not favor the diffusion of the supported species into the vacancy-containing spinel structure of the alumina (main component of the support). Table 4 also includes the surface concentration of Ru(0). The surface metallic ruthenium content is of interest for calculating the activity parameters of the catalysts, since the metallic sites have the function of activating H_2. In this sense, it should be noted that the Ru3/ZA and Ru5/ZA catalysts are the samples with the highest surface concentration of zerovalent species. However, the former is the most active of the catalysts tested, as shown in Fig. 1a. In terms of surface concentration, in this sample ruthenium is more dispersed on the surface (Ru/Zr=0.45 for the Ru3/ZA catalyst vs. Ru/Zr=1.85 for the Ru5/ZA catalyst), which is another feature that should be taken into account when explaining the better performance of the Ru3/ZA system. On the other hand, the stability of the reduced particles is also worth noting since the catalysts maintain their composition after being exposed to air at room temperature for long periods of time and do not need to be pre-reduced before carrying out the catalytic measurements. A similar result was found by Z. Wei et al. with Ru/N-doped hierarchically porous carbon catalysts.[40]

The catalyst´s acid properties were probed by NH_3-TPD. Table 5 shows the amount of NH_3 desorbed per gram of catalyst in the 100–300°C, 300-500°C, and 500-800°C temperature ranges. The 100-300°C range is associated with weak acidity, the 300-500°C range with medium acidity, and the last one with strong acidity.[38]

The Ru1.5/ZA and Ru3/ZA samples have a higher NH_3 adsorption capacity than the Ru0.5/ZA catalyst, indicating that they contain a greater number of acid sites and also have a high number of medium and strong acid sites. These sites are probably associated with the presence of oxidic ruthenium species, mainly Ru(III) and Ru(IV), as evidenced by XPS results, which can generate Lewis-type acid sites.

Table 5. NH_3-TPD results in mmol NH_3 desorbed per gram of catalyst for reduced samples.

Temperature Range	Ru0.5/ZA	Ru1.5/ZA	Ru3/ZA
100-300°C	0.15	0.69	0.44
300-500°C	0.47	0.59	0.72
500-850°C	0.27	0.43	0.33
Total	0.89	1.71	1.49

Table 4. Surface elemental concentrations determined by XPS.

Catalyst	wt.%						Atomic ratio	
	C1s	O 1*s*	Ru 3*p*	Al 2*p*	Zr 3$d_{5/2}$	Ru(0)	Ru/Zr (XPS)	Ru/Zr (nominal)
Ru0.5/ZA	10.92	45.07	1.37	34.37	8.27	1.10	0.15	0.04
Ru1.5/ZA	13.28	42.39	3.15	30.62	10.56	2.36	0.27	0.12
Ru3/ZA	20.05	34.87	7.41	22.9	14.78	5.41	0.45	0.25
Ru5/ZA	33.84	23.70	10.12	27.38	4.94	7.18	1.85	0.41

Structure-performance correlation discussion

Below are some points that can be used to establish a correlation between the catalytic performance of the catalysts and their physicochemical properties. This analysis assumes that the mechanism of this reaction requires two types of sites for the reaction to succeed: metal sites and acid sites. According to the data presented in Fig.1 and the results obtained from the physicochemical characterization of the catalysts, the activity increases as the surface ruthenium concentration increases from 0.5 to 3 wt.%. Subsequent addition of ruthenium results in a less active catalyst, probably due to surface segregation of the metallic phase (Ru/Zr ratio higher than expected) and, apparently, to a lower dispersion of the active phase. Calculation of the initial reaction rate confirms that the Ru3/ZA catalyst is the most active one (Table 6).

Table 6. Conversion, selectivity, and initial reaction rate for catalysts studied.

Catalyst	X_{LA} (%)	S_{GVL} (%)	mmolLA/mmolRu$_{sup}$*s[a]	mmolLA/mmolRu^0*s[b]
Ru0.5/ZA	70	97.4.	0.31	0.38
Ru1.5/ZA	98	99.4	0.76	0.98
Ru3/ZA	99	99.9	0.78	1.07
Ru5/ZA	97	98.8	0.27	0.19

Reaction conditions: 0.1 g of catalyst; T: 120 ºC; P: 30 bar H_2; time: 1 h of reaction. [a] Initial rate per mmol of surface ruthenium (by XPS). [b] Initial rate per mmol of zerovalent ruthenium (by XPS).

Results obtained with the more dispersed catalysts are similar to and quite higher than those reported by Piskun et al. with titania-supported ruthenium catalysts[31] and by Yan et al. with silica-supported palladium catalysts. These authors observed that increasing the metallic load increased the turnover number (TON).[41] In contrast, Primo et al. reported that by increasing the ruthenium content in catalysts supported on titania, a decrease in TOF was obtained.[42] It is evident, therefore, that there are different factors intrinsic to the catalysts that determine their activity. One of those intrinsic factors that can condition the catalytic activity is the nature of the ruthenium-supported phases. When analyzing the results presented in this work, a correlation is observed between the catalytic activity and the surface composition of the catalysts, determined by XPS. Thus, it is possible to find a linear correlation between the Ru(0)/Ru(III) ratio and the initial rate of the reaction, expressed in $mmol_{LA}/g_{RuSup}$*s (Fig. S6), as long as the ruthenium concentration remains less than or equal to 3 wt.%. Although very good catalytic results with ruthenium-based catalysts have been reported in the literature, the high LA conversions achieved in this work, which were also obtained at very low reaction times, are noteworthy. Table 7 compares the results obtained in this work with others reported in the bibliography. The results presented suggest that under the experimental conditions used, which can be considered medium pressure and temperature, highly promising results have been achieved in terms of conversion of LA, especially considering that it is a catalytic system based on the use of a low-cost support.

Table 7. Comparison of the catalytic results obtained in this work with others reported in the literature.

Catalyst	LA/Ru molar ratio (nominal)	PH_2 (bar)	T (°C)	t (h)	Conversion (%) / Yield	Ref.
Ru0.5/ZA	4851	30	120	1	70/ 68.1	This work
Ru1.5/ZA	1617	30	120	0.5	98/ 97.4	This work
Ru3/ZA	809	30	120	0.5	99.0/ 98.9	This work
Ru/PNC-I	320	10	30	3.5	97.8/ 96.8	[45]
Ru(3)/NHPC	337	10	50	3	>99/>99	[40]
Ru(4)/AlZr	825	15	120	6	100/ 100	[43]
Ru(1)/TiO_2	4353	40	130	0.5	100/ 99.9	[34]
Ru(1)/TiO_2	4350	45	90	4	86/ 79	[31]
Ru(1)/OMS	3851	30	100	1	99.9/ 99.8	[46]
Ru(5)/Z	2100	24	130	2	99/ 99.8	[47]

Regarding the catalytic selectivity of the Rux/ZA catalysts (Fig. 1b and Table 6), GVL was obtained as the main product. It is worth mentioning that a high selectivity was reached even when the conversion did not reach its maximum value. For example, with the Ru0.5/ZA catalyst, the conversion achieved at 1 h was 70% and the selectivity to GVL was 99%. As a by-product, it was

possible to detect the presence of 4-hydroxypentanoic acid (HPA) in very low concentration. The results of the variation of LA concentration and the reaction products as a function of time for three tested catalysts are presented in the Supplementary Material (Figure S7), where the characteristics of the reaction intermediate of HPA can be seen. This by-product was also found by other authors working under similar conditions.[31,43]

Under the pressure and temperature conditions used to obtain the results presented in this work, the system is heterogeneous, formed by a liquid phase and the catalytic solid. According to bibliographic reports, in the liquid phase the prevailing reaction mechanism is the one whose first step is the hydrogenation of the keto-carbonyl group of LA to form 4-hydroxypentanoic acid.[44] This reaction step is favored by the presence of highly dispersed metal ruthenium nanoparticles on the catalytic surface. In this sense, in a recent work it has been shown that the formation of GVL from the hydrogenation of LA and alkyl levulinate can occur through a noncompetitive Langmuir-Hinshelwood mechanism where the substrates and H_2 are adsorbed on different sites.[48] Moreover, there are reports that indicate that the greater the rate of the hydrogenation reaction from LA to GVL the smaller the size of the metallic particle.[31,35,43] This same trend was observed by Primo et al. who found that increasing the size of TiO_2-supported metal Ru nanoparticles, from 2 nm to 10 nm, substantially decreased the efficiency of the catalysts in the lactic acid hydrogenation reaction.[42] The Ru0.5/ZA, Ru1.5/ZA and Ru3/ZA catalysts studied contain very small ruthenium particles (< 5 nm), therefore the higher activity found with the Ru3/ZA catalyst in terms of higher initial velocity could be associated with the greater number of small metallic particles present in this system. In the same sense, Cao et al. showed that carbon was a better support for the selective synthesis of GVL as compared to alumina due to the high number of metallic Ru particles formed on that support.[49] Although the metal particle size of the Ru5/ZA catalyst was not determined by TEM, the lower dispersion of the metal phases supported in this catalyst, suggested by XPS, indicates the segregation of ruthenium, being this fact responsible for the notable loss of the initial rate.

In addition, it has been reported that ruthenium would have the role of helping to reduce the energy gap of the reaction pathway due to its ability to generate H-bonded water molecules or single chemisorbed water on Ru surface.[40,50,51] Hydrogen atoms of water molecules would take part in the hydrogenation of the C=O group of LA, promoting the catalytic activity and the yield to GVL.

The promoting effect of Zr on the ruthenium catalytic system cannot be neglected. First, the presence of Zr on the support favors the formation of zerovalent Ru particles compared to Al_2O_3, as verified by XPS (see Supplementary Material, Table S1). On the other hand, it has been proposed that there is an SMSI effect between the Zr and Ru species, with a charge transfer towards the metallic sites. This would generate a greater electronic density on the Ru atoms and therefore, a greater capacity of the system to adsorb and activate both the substrate through its carbonyl bond and the hydrogen molecule.[43]

It has also been reported that the presence of acid sites could favor the adsorption of the substrate (LA).[52] In this sense, the two most active samples (Ru1.5/ZA and Ru3/ZA) are those with the highest number of acid sites of medium and high strength, which would indicate that the presence of some oxidized species of ruthenium could be involved in the reaction mechanism and that the systems studied in this work present a certain bifunctionality.

Influence of different operational variables on obtaining GVL with the Ru3/ZA catalyst

Several investigations conducted on the hydrogenation reaction of LA to give GVL showed that the efficiency of the catalysts depends on the reaction conditions used. Some of the most influencing factors are reaction temperature, H_2 pressure, LA/catalyst mass ratio, and reaction time. As Ru3/ZA showed the best catalytic activity under the selected reaction conditions, in terms of the highest initial rate, this catalyst was chosen for the study of the effect of the mentioned factors on the activity and selectivity towards GVL.

Effect of temperature and pressure

The effect of temperature on the catalytic performance in the hydrogenation of LA to GVL was studied by varying the reaction temperature between 25 and 150°C. Specifically, the conversion at 1 h of reaction was measured at 25, 40, 80, 100, 120, and 150°C, and the results are shown in Fig. 7. At room temperature the conversion achieved is low (<15%). An increase in temperature up to 100°C generates a significant increase in conversion. The highest conversion is reached at a temperature of 120°C and from this value on the conversion remains constant. Regarding the selectivity to GVL, it was always above 80% for all the temperatures evaluated. It is worth mentioning that at 150°C there is a slight decrease in selectivity compared to the value at 120°C. This can be attributed to the breaking of certain bonds of the GVL molecule under these thermal conditions.

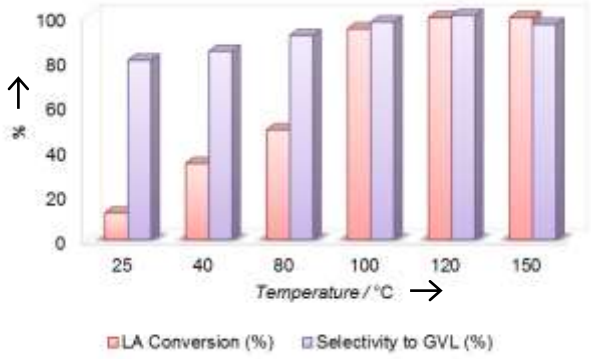

Figure 7. Hydrogenation of LA to GVL: influence of temperature on the conversion of LA and the selectivity to GVL.

The effect of pressure on the conversion of LA to GVL was studied using 5, 10, 20 and 30 bar of H_2 in the presence of the Ru3/ZA catalyst at 120°C (Fig. 8). From the results obtained, it can be concluded that activity increases with pressure. As far as the selectivity is concerned, it increases with the H_2 pressure and is close to 100% at the highest pressures used.

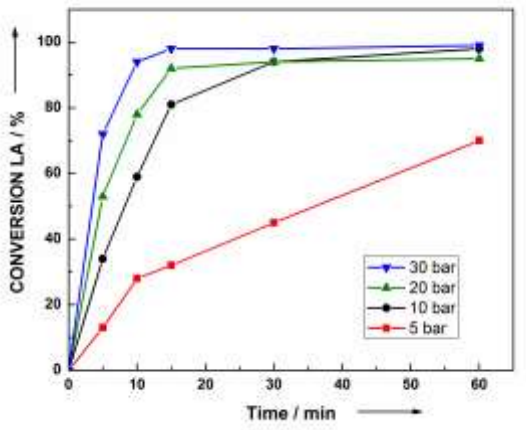

Figure 8. Effect of pressure on the conversion of LA for Ru3/ZA catalyst.

Catalyst mass effect

First of all, it should be mentioned that in the absence of a catalyst, no conversion of LA to GVL was observed after 1 h of reaction. The results of the experiments carried out with different catalyst masses are shown in Fig. 9. It can be seen that almost 100% conversion was reached after 15 min of reaction when working with both 0.1 g and 0.05 g of Ru3/ZA catalyst. This was not the case in the experiment conducted with 0.025 g of catalyst, where at 15 min the conversion of LA was 45%.

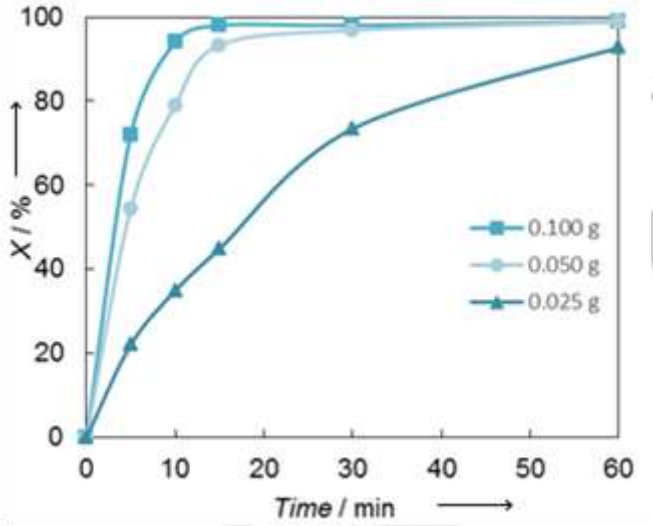

Figure 9. Conversion of LA to GVL as a function of time using different masses of Ru3/ZA catalyst.

All these tests corroborate that the operating conditions selected in this work (120°C, 30 bar of H_2, 0.1 g of catalyst, and 1 h of reaction) are the best within the group of values studied.

Reuses and characterization of the reused catalyst

To evaluate the stability of the Ru3/ZA catalyst after reuse cycles, recovery and reuse experiments were performed. To carry out these tests, the catalyst used in the reaction was separated from the medium by centrifugation, washed, dried, and reused. The results shown in Fig.10 indicate that the Ru3/ZA catalyst maintained high activity and selectivity values after its reuse.

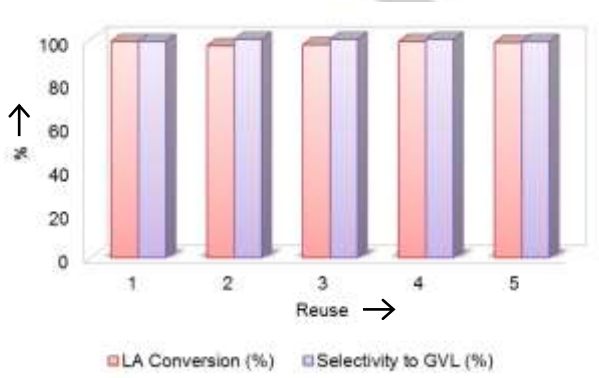

Figure 10. Conversion of LA and selectivity to GVL in reusing Ru3/ZA catalyst

It is evident that there has been no significant change in the nature of the active phase and/or the composition of the catalyst during the reaction. This statement is supported by the catalytic results and the characterization of the Ru3/ZA catalyst used in five reaction cycles (Table 8). Comparing the results obtained by XPS for the fresh and post-reaction catalyst, only a slight enrichment of the Ru(0) fraction is observed, at the expense of the Ru(IV) fraction. Likewise, a slight increase in the size of the metallic particle was observed, according to the results obtained by TEM. These results are highly promising, since it was not necessary to use complex regeneration procedures before each use, the recovered catalyst was only washed, dried, and weighed before reuse.

Table 8. XPS and TEM characterization of Ru3/ZA catalyst fresh and after five catalytic runs

	Ru3/ZA catalyst	
	Fresh	After 5 catalytic runs
	BE (EV)	
Ru 3$p_{3/2}$	Ru (0) 461.9 (73) Ru (III) 464.4 (22) Ru (IV) 466.3 (5)	Ru (0) 461.5 (79) Ru (III) 464.4 (21) Ru (IV) 466.1 (0)
C1*s*	284.8	284.9
O 1*s*	531.0	531.0
Al 2s	74.3	74.2
Zr 3$d_{5/2}$	181.9	181.8
Ru/Zr atomic ratio	0.45	0.51
d_{TEM} (nm)	2.4	3.1

Conclusions

To summarize, in this work, the results related to the in-depth characterization and the catalytic performance of zirconia-alumina supported Ru catalysts have been presented. All the studied catalysts were active, selective, and stable in the aqueous phase hydrogenation of LA to GVL under the mild experimental conditions evaluated. The initial reaction rate was found to depend on the ruthenium concentration. Therefore, the Ru3/ZA catalyst showed the highest activity, obtaining high levels of conversion and selectivity towards GVL at low reaction times (<30 min). This was attributed to the higher amount of small size (around 2.4 nm) metallic ruthenium particles in this catalyst. The role of ruthenium was associated with the activation of H_2 and of the carbonyl group of LA, which favored the initial hydrogenation stage of the reaction mechanism, giving the intermediate 4-hydroxypentanoic acid. Nevertheless, the results found support the idea that the catalytic activity not only depends on the metallic Ru(0) active sites, but those properties attributed to the oxidic species present in the catalysts, coming from ruthenium, zirconium and aluminum oxides, must also be taken into account. These species supply acid sites to the system, contributing to its good performance. The Ru3/ZA catalyst, in addition to exhibiting very good activity and selectivity, showed very good stability after successive cycles of use without the need for regeneration in between.

Experimental Section

Chemicals

Chemical reagents purchased from reputable companies were used as received, without further purification. $ZrOCl_2.8H_2O$ (reagent grade 98%) and levulinic acid were purchased from SIGMA-ALDRICH. $RuCl_3.xH_2O$ was purchased from Merck, and alumina (γ-Al_2O_3) from Air Products. H_2 and He gases used in the work were of high purity.

Preparation of the zirconia-alumina support

Zirconia-alumina support (ZA) was synthesized by the sol-gel method. A suspension of Al_2O_3 and the amount of $ZrOCl_2{\cdot}8H_2O$ necessary to obtain 15 wt.% of ZrO_2 on Al_2O_3 in Milli-Q water was prepared, according to the procedure followed by Jaworski et al.[35] The mixture was kept under stirring at room temperature, and aqueous ammonia (ca. 1 M) was added until the pH of the solution reached a value of 10 and gel formation was observed. The gel underwent an aging process for 7 days. The white precipitate obtained was washed with Milli-Q water until it was verified that the filtrate was free of chloride ions (determined by $AgNO_3$) and dried at 105°C for 24 h. The resulting solid was calcined at 600°C for 2 h.

Preparation of Rux/ZA catalysts

For the preparation of the Rux/ZA catalysts, the wet impregnation technique was employed, using a liquid to solid ratio of 5:1. In a typical procedure, 2 g of the ZA support was contacted with 10 mL of a solution containing the appropriate amount of $RuCl_3.xH_2O$ to obtain x wt% Ru in the final catalyst (x = 0.5, 1.5, 3 and 5). The systems were left in contact for 24 h in a covered container, and then were dried in an oven at 105°C for 24 h. Before being used in the reaction, the precursors were reduced at 300°C for 2 h in an H_2 flow, and the chloride present was removed by washing them with Milli-Q water until negative reaction of chlorides with silver nitrate. The catalysts were named Rux/ZA, with x being the nominal Ru content.

Characterization of the support and catalysts

The textural properties of the ZA support were studied by nitrogen physisorption, obtaining the N_2 adsorption-desorption isotherms at -196 °C, in Micromeritics ASAP 2020 equipment. The BET method (SBET) was used to obtain the specific surface area, and the pore volume (Vp) was estimated using the adsorption branch of the isotherm.
Scanning electron microscopy (SEM) analysis was conducted on a FEI Quanta200 microscope coupled with an SDD Apollo 40. EDS elemental mapping images were also obtained.
For the identification of the crystalline species present in the support and the catalysts, X-ray diffraction studies (XRD) were conducted. The analyses were performed at the Centralized Research Support Services (SCAI) of the University of Malaga (Spain), using an EMPYREAN PANalytical diffractometer consisting of an automatic loader and rotating sample holder. Measurements were made from 4° to 70° (2θ) for 5 min, with a step size of 0.0167°. The X-ray tube was operated at 45 kV and 40 mA, and the sample was rotated at 10 rpm during the measurement.
Temperature programmed reduction (TPR) experiments were performed with a 5% H_2/Ar mixture in laboratory-built equipment, from 25 to 800°C with a heating rate of 10°C/min. The mass of catalyst used in each experiment was 50 mg. A Shimadzu GC-8A gas chromatograph equipped with a TCD detector was used for measuring hydrogen consumption.
NH_3-TPD was performed on Micromeritics AutoChem 2910 equipment. In a typical experiment, a 30 mg sample loaded in the reactor was treated at atmospheric pressure with a He flow of 60 mL min^{-1} from room temperature to 800°C, and keeping this temperature for 15 min. After cooling to 100°C, NH_3 adsorption was carried out by switching He to a 10% NH_3-He (in vol.) mixed gas and then keeping for 30 min. The physisorbed NH_3 was purged with He at 100°C. Finally, TPD was then conducted in He flow by raising the temperature to 800°C at a rate of 10 °C min^{-1}.
Transmission electron microscopy (TEM) images were obtained using a TEM Talos F200X instrument and a TEM/STEM FEI TECNAI F20 microscope with an acceleration voltage of 200 kV. The powder samples were suspended in ethanol and treated by ultrasound for 15 min. Then, a drop of the suspension was deposited on a Quantifoil® carbon film supported by a grid of Cu and dried before analysis. TEM images were analyzed with the Digital Micrograph software. Histograms of the particle size distribution were constructed counting at least 200 particles.
XPS experiments on both fresh and used catalysts were performed on PHI Versa Probe II Scanning XPS Microprobe with scanning monochromatic X-ray Al Kα radiation as the excitation source (200 μm diameter analyzed, 25.0 W, 15 kV, 1486.6 eV), and a charge neutralizer. The pressure in analysis chamber was kept lower than 2.0×10^{-6} Pa. High-resolution spectra were recorded at a given take-off angle of 44° by a multichannel hemispherical electron analyzer operating in the constant pass energy mode at 29.35 eV. Spectra were charge referenced with the C 1*s* of adventitious carbon at 284.8 eV. Energy scale was calibrated using Cu $2p_{3/2}$, Ag $3d_{5/2}$, and Au $4f_{7/2}$ photoelectron lines at 932.7, 368.2, and 83.95 eV, respectively. The Multipack software version 9.6.0.15 was employed to analyze the recorded spectra. The obtained spectra were fitted using Gaussian–Lorentzian curves. The samples were measured as received in the laboratory, without any special pretreatment.

Catalytic tests

The tests were carried out in an autoclave type reactor (Berghof BR 100, 100 mL). A volume of 40 mL of an aqueous solution 0.6M of levulinic acid was used in each test. Unless otherwise said, the following conditions were used: a temperature of 120°C, an H_2 pressure of 30 bar, a mass of catalyst of 0.1 g, and water as solvent. The reaction time was 60 min. The products were analyzed using samples taken during the reaction by gas chromatography on a SHIMADZU GC-2014 gas chromatograph with a flame ionization detector (FID) and a Supelco SPBTM-5 capillary column (30 m x 0.25 mm x 0.25 µm). The products were identified by a gas chromatography−mass spectrometry technique (GC-MS), using SHIMADZU CG-MS QP2010 SE equipment and a Supelco SPBTM-5 column (30 m × 0.25 mm × 0.25 µm).

LA conversion (X_{LA}) was followed by analyzing the decrease in the concentration of LA and calculated according to the following expression:

$$X_{LA}^{t}(\%) = \frac{C_{LA}^{0} - C_{LA}^{t}}{C_{LA}^{0}} . 100$$

where C_{LA}^{0} is the initial LA concentration in the reactor and C_{LA}^{t} is the LA concentration at the reaction time t. Selectivity to GVL (S_{GVL}^{t}) was calculated according to:

$$S_{GVL}^{t} = \frac{C_{GVL}^{t}}{C_{LA}^{0} - C_{LA}^{t}} . 100$$

where C_{GVL}^{t} is the concentration of GVL at the reaction time t.

Inter- and intra-particle diffusional limitations were verified to be negligible, as informed in the Supplementary Material.

In the recycling experiments, the Ru3/ZA catalyst used at 120°C and 30 bar of H_2 for 1 h of reaction was separated by centrifugation, washed with Milli-Q water, dried in an oven at 60°C for 2 h, and reused. The same recycling procedure was repeated in the subsequent uses. The LA/catalyst mass ratio was kept constant in all the experiments.

Acknowledgements

The authors would like to acknowledge the following institutions of Argentina for the financial support, UNNOBA (project SIB 2022 and project PPIC UNNOBA EXP 2703/2019), UNLP (project X903, Expte 100-1282/19), CONICET (project PUE 005/2018, EXP. 8085/17; PIP 086/2022 and PIP 0134/2021) and ANPCyT FONCyT (PICT 2019/1962), M.M, E.R.A., J.A.C and E.R.C thank Ministerio de Ciencia e Innovación, project PID2021-126235OB-C32, and Junta de Andalucía, project P20_00375 and FEDER funds.

Keywords: levulinic acid • γ-valerolactone • ruthenium catalysts • hydrogenation • XPS

References

[1] D.M. Alonso, S.G. Wettstein, J.A. Dumesic, *Green Chem.* **2013**, *15*, 584–595.

[2] P. Gallezot, *Chem. Soc. Rev.* **2012,** *41,* 1538-1558.

[3] X. Xu. Y. Li. Y. Gong. P. Zhang. H. Li. Y. Wang, *J. Am. Chem. Soc.* **2012**, *134,* 16987-16990.

[4] S. S. Chen, T. Maneerung, D. C. W. Tsang, Y.S. Ok, C-H. Wang, *Chem. Eng. J.* **2017**, *328*, 246-273.

[5] D. Resasco. S. Sitthisa. J. Faria. T. Prasomsri. M. P. Ruiz, in *Heterogeneous Catalysis in Biomass to Chemicals and Fuels*, (Eds: David Kubička and Iva Kubičková) **2011**, Ch. 5. Kerala, India: Research Signpost.ISBN: 978-81-308-0462-0.

[6] J. J. Bozell, G. R. Petersen, *Green Chem.* **2010**, *12,* 539–554.

[7] S. Takkellapati, T. Li, M. A. Gonzalez, *Clean Technol. Environ. Policy.* **2018**, *20(7)*, 1615–1630.

[8] M. Chalid, H.J. Heeres, A.A. Broekhuis, *J. Appl. Polym. Sci.* **2012**, *123*, 3556-3564

[9] J.Q. Bond, D.M. Alonso, R.M. West, J.A. Dumesic, *Langmuir* **2010**, *26*, 16291-16298.

[10] H. Mehdi, V. Fábos, R. Tuba, A. Bodor, L. T. Mika, I. T. Horváth, *Top. Catal.* **2008**, *48*, 49–54.

[11] L. Ye, Y. Han, J. Feng, X. Lu, *Ind. Crops Prod.* **2020**, *144*, 112031.

[12] E.V. Starodubtseva, O.V. Turova, M.G. Vinogradov, L.S. Gorshkova, V.A. Ferapontov, *Russ. Chem. Bull.* **2005**, *54*, 2374–2378.

[13] W. R. H. Wright, R. Palkovits, *ChemSusChem* **2012**, *5*, 1657 – 1667.

[14] P. Upare, J.-M. Lee, D. W. Hwang, S. B. Halligudi, Y. K. Hwang, J.-S.Chang, *J. Ind. Eng. Chem.* **2011**, *17*, 287 – 292.

[15] J. J. Bozell, L. Moens, D. C. Elliott, Y. Wang, G. G. Neuenscwander, S. W.Fitzpatrick, R. J. Bilski, J. L. Jarnefeld, *Resour., Conserv. Recycl.* **2000**, *28*, 227 – 239.

[16] B. Putrakumar, N. Nagaraju, V.P., Kumar, K.V.R. Chary, *Catal.Today* **2015**, *250*, 209–217.

[17] D. Sun, Y. Takahashi, Y. Yamada, S. Sato, *Appl. Catal., A* **2016**, *526,* 62-69.

[18] S. Lomate, A. Sultana, T. Fujitani, *Catal. Lett.* **2018**, *148* 348-358.

[19] L. Forrer Sosa, V. Teixeira da Silva, P. M. de Souza. *Catal. Today* **2021**, *381*, 86–95.

[20] A. Hijazi, N. Khalaf, W. Kwapinski, J. J. Leahy. *RSC Adv.* **2022**, *12*, 13673-13694.

[21] H.C. Genuino, H.H. van de Bovenkamp, E. Wilbers, J.G.M. Winkelman, A. Goryachev, J.P. Hofmann, E.J.M. Hensen, B.M. Weckhuysen, P.C.A. Bruijnincx, H.J. Heeres. *ACS Sust. Chem. Eng.* **2020**, *8 (15),* 5903–5919.

[22] A. García, R. Sánchez-Tovar, P. J. Miguel, E. Montejano-Nares, F. Ivars-Barceló, J. A. Cecilia, B. Torres-Olea, B. Solsona. *Fuel* **2023**, *352,* 129045.

[23] S. Dutta, I. K. M. Yu, D. C. W. Tsang, Y. H. Ng, J. H. Clark, *Chem. Eng. J.* **2019**, *372*, 992-1006.

[24] F. liguori, C. Moreno-Marrodan, P. Barbaro, *ACS Catal.* **2015**, *5*, 1882-1894.

[25] J.J. Musci, M. Montaña, E. Rodríguez-Castellón, I.D. Lick, M.L. Casella, *Mol. Catal.* **2020**, *495,* 111150.

[26] M. Nemanashi, J.-H. Noh, R. Meijboom, *Appl. Catal., A* **2018**, *550*, 77-89.

[27] W. Luo, M. Sankar, A.M. Beale, Q. He, C.J. Kiely, P.C.A. Bruijnincx, B.M. Weckhuysen, *Nat. Commun.* **2015**, *6*, 6540.

[28] W. Luo, U. Deka, A.M. Beale, E.R.H. van Eck, P.C.A. Bruijnincx, B.M. Weckhuysen, *J. Catal.* **2013**, *301,* 175-186.

[29] M.G. Al-Shaal, W.R.H. Wright, R. Palkovits, *Green Chem.* **2012**, *14*, 1260-1263.

[30] D. Ding, J. Wang, J. Xi, X. Liu, G. Lu, Y. Wang, *Green Chem.* **2014**, *16,* 3846-3853.

[31] A. S. Piskun, J. Ftouni, Z. Tang, P.C.A. Bruijnincx, H.J. Heeres, *Appl. Catal., A* **2018**, *549*, 197-206.

[32] M. Wąchała, J. Grams, W. Kwapiński, A. M. Ruppert, *Int. J. Hydrogen Energy* **2016**, *41*, 8688-8695.

[33] A. Aboulayt, T. Onfroy, A. Travert, G. Clet, F. Maugé, *Appl. Catal., A* **2017**, *530,* 193-202.

[34] J. Tan. J. Cui. T. Deng. X. Cui. G. Ding. Y. Zhu. Y. Li. *ChemCatChem* **2015**, *7*, 508-512.

[35] M. Thommes, K. Kaneko, A.V. Neimark, J.P. Olivier, F. Rodriguez-Reinoso, J. Rouquerol et al. Physisorption of gases, with special reference to the evaluation of surface area and pore size distribution (IUPAC Technical Report) 87 9-10 2015 1051 1069 10.1515/pac-2014-1117.

[36] M.A. Jaworski, I.D. Lick, G.J. Siri, M.L. Casella, *Appl. Catal. B Environ.* **2014**, *156-157*, 53-61.

[37] H. Seok Whang, M. Seok Choi, J. Lim, C. Kim, I. Heo, T.S. Chang, H. Lee, *Catal. Today* **2017**, *293–294*, 122–128.

[38] J. J. Musci, M. Montana, A. B. Merlo, E. Rodríguez-Aguado, J. A. Cecilia, E. Rodríguez-Castellon, I. D. Lick, M. L. Casella *Catal.Today* **2022**, *394-396*, *81-93.*

[39] P. Braos-García, C. García-Sancho, A. Infantes-Molina, E. Rodríguez-Castellón, A. Jiménez-López, *Appl. Catal., A* **2010**, *381*, 132–144.

[40] Z. Wei, X. Li, J. Deng, J. Wang, H. Li, Y. Wang, *Mol. Catal.* **2018**, *448*, 100-107.
[41] K. Yan, T. Lafleur, G. Wu, J. Liao, Ch. Ceng, X. Xie, *Appl. Catal., A* **2013**, *468*, 52– 58.
[42] A. Primo, P. Concepción, A. Corma, *Chem. Commun.* **2011**, *47*, 3613–3615.
[43] Y. Lu, Y. Wang, Y. Wang, Q. Cao, X. Xie, W. Fang, *Mol. Catal.* **2020**, *493*, 111097.
[44] O.A. Abdelrahman, A. Heyden, J.Q. Bond, *ACS Catal.* **2014**, *4*, 1171–1181.
[45] J. Yang, R. Shi, G. Zhou, *Chem. Eng. J.* **2023**, *475*, 146297.
[46] J. Molleti, M. S. Tiwari, G. D. Yadav, *Chem. Eng. J.* **2018**, *334*, 2488–2499.
[47] B. C. Filiz, E. S. Gnanakumar, A. Martínez-Arias, R. Gengler, P. Rudolf, G. Rothenberg, N. Raveendran Shiju, *Catal. Lett.* **2017**, *147*, 1744–1753.
[48] J.Delgado, W. N. Vasquez Salcedo, G. Bronzetti, V. Casson Moreno, M. Mignot, J. Legros, C. Held, H. Grénman, S. Leveneur, *Chem. Eng. J.* **2022**, *430, 3*, 133053.
[49] S. Cao, J.R. Monnier, C.T. Williams, W. Diao, J.R. Regalbuto, *J. Catal.* **2015**, *326*, 69–81
[50] C. Michel, J. Zaffran, A. M. Ruppert, J. Matras-Michalska, M. Jędrzejczyk, J. Grams, P. Sautet, *Chem. Commun.* **2014**, *50*, 12450-12453.
[51] C. Michel, P. Gallezot, *ACS Catal.* **2015**, *5*, *7*, 4130–4132.
[52] L. Corbel-Demailly, B.-K. Ly, D.-P. Minh, B. Tapin, C. Especel, F. Epron, A. Cabiac, E. Guillon, M. Besson, C. Pinel, *ChemSusChem* **2013**, *6*, 2388–2395.

Graphical Abstract

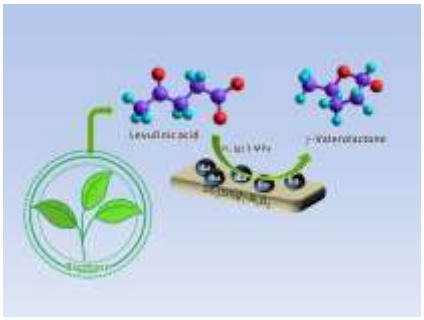

Table of Contents. Catalytic upgrading of levulinic acid is highly relevant in biorefinery and heterogeneous catalysis. A 3 wt.% Ru catalyst supported on zirconia-alumina efficiently and selectively converted levulinic acid to γ-valerolactone under mild reaction conditions and using water as solvent. The catalyst was tested in five consecutive cycles, keeping its activity and selectivity. Characterization provided valuable insight into physicochemical properties and catalytic performance.